A gyro-kinetic model for trapped electron and ion modes

Thomas Drouot, Etienne Gravier, Thierry Réveillé, Alain Ghizzo, Pierre Bertrand, Xavier Garbet, Yanick Sarazin, Thomas Cartier-Michaud

A gyro-kinetic model for trapped electron and ion modes[s]

Thomas Drouot[1,a], Etienne Gravier[1], Thierry Reveille[1], Alain Ghizzo[1], Pierre Bertrand[1], Xavier Garbet[2], Yanick Sarazin[2], and Thomas Cartier-Michaud[2]

[1] IJL, UMR 7198 CNRS, Université de Lorraine, 54500 Vandoeuvre-les-Nancy, France
[2] CEA, IRFM, 13108 Saint-Paul-Lèz-Durance Cedex, France

Received 27 February 2014 / Received in final form 10 June 2014
Published online 1 October 2014 – © EDP Sciences, Società Italiana di Fisica, Springer-Verlag 2014

Abstract. In tokamak plasmas, it is recognized that ITG (ion temperature gradient instability) and trapped electron modes (TEM) are held responsible for turbulence giving rise to anomalous transport. The present work focuses on the building of a model including trapped kinetic ions and trapped kinetic electrons. For this purpose, the dimensionality is reduced by averaging the motion over the cyclotron motion and the "banana" orbits, according to the fact that the instabilities are characterized by frequencies of the order of the low trapped particle precession frequency. Moreover, a set of action-angle variables is used. The final model is 4D (two-dimensional phase space parametrized by the two first adiabatic invariants namely the particle energy and the trapping parameter). In this paper, the trapped ion and electron modes (TIM and TEM) are studied by using a linear analysis of the model. This work is currently performed in order to include trapped electrons in an existing semi lagrangian code for which TIM modes are already taken into account. This study can be considered as a first step in order to include kinetic trapped electrons in the 5D gyrokinetic code GYSELA [J. Abiteboul et al., ESAIM Proc. **32**, 103 (2011)].

1 Introduction

Low frequency turbulence developing from micro instabilities is responsible for the phenomenon of anomalous radial energy transport in magnetically confined fusion plasmas. Among these instabilities, ion temperature gradient (ITG), interchange instabilities, and trapped electron modes (TEM) may play an important role in explaining the anomalous heat and particle transport observed in tokamaks. These instabilities are driven by ion and electron equilibrium gradients [1–4]. ITG seems to be responsible of the anomalous ion heat transport whereas the TEM turbulence drives electron particle and heat transport, and their interactions may play a non-negligible role in determining the whole properties of turbulent plasma transport [5]. Considering a model with trapped kinetic ions and electrons allows one to cover both TIM/TEM regimes simultaneously. These instabilities are characterized by frequencies of the order of the trapped particle precession frequency, and their influence on anomalous transport is still under discussion.

The present paper focuses on the building of a 4D reduced model including trapped kinetic ions and electrons. The linear analysis of this model is performed. The paper is organized as follows.

Section 2 presents the motion of a charged particle in a tokamak. It can be noticed that this motion is integrable and can be divided into three parts: the cyclotron motion which consists of a fast rotation around the magnetic field lines, a "banana" like shape poloidal motion and a toroidal precession. Thus, in agreement with classical mechanics, it is interesting to use a set of action-angle variables where angles are related to these periodic motions and actions are three invariants related to the magnetic moment μ, the energy E and the toroidal kinetic momentum M. In this framework the Hamiltonian at the equilibrium only depends on actions so that using these coordinates provides great simplifications. In addition, the dimensionality is reduced by averaging the motion over the cyclotron motion and the "banana" orbits, according to the fact that the instabilities are characterized by frequencies of the order of the low trapped particle precession frequency.

The kinetic model for TEM and TIM instabilities is addressed in Section 3. It is a model parametrized by the two first adiabatic invariants namely the particle energy and the trapping parameter (or pitch angle). Vlasov equations are much easier to solve using such a model.

The quasi-neutrality constraint is used to ensure the self consistency of the model. This constraint is the main source of difficulties of the model for two reasons. Firstly the model dealing with the bounce averaged distribution function allows us to calculate the "banana" density whereas the quasi-neutrality constraint requires the particle density. The derivation of the polarization term is

[s] Contribution to the Topical Issue "Theory and Applications of the Vlasov Equation", edited by Francesco Pegoraro, Francesco Califano, Giovanni Manfredi and Philip J. Morrison.

[a] e-mail: thomas.drouot@univ-lorraine.fr

required to obtain the particle density. Secondly, the density is obtained by integrating the distribution function over the velocity which no longer appears in the model but which is a nontrival function of action-angle variables. In spite of this additional complexity, the gyro-bounce-averaged approach which is detailed in this paper remains numerically competitive as compared to the gyrokinetics approach to address the physics of trapped modes. Indeed, the complex expression of the quasi-neutrality does not annihilate the gain obtained by reducing the phase space from 5 to 4 dimensions.

Finally, the results of the linear analysis of the model are given in Section 4. Analytic dispersion relations are derived and discussed. The behavior of both TIM and TEM is studied for different toroidal mode numbers.

2 Single particle motion in a tokamak

This section outlines the orbit of a single particle in a prescribed magnetic field of a tokamak. In particular we focus on the development to obtain the characteristic frequencies of the system. These frequencies allow the reduction dimensionality of the problem and the possibility of including electrons. Note that a more detailed development of the model is given in [6] for ion species.

2.1 Magnetic configuration

In order to derive the kinetic model describing the trapped electron and ion modes in a Tokamak, we assume an axisymetric magnetic toroidal configuration and use the Boozer-Clebsch representation of the magnetic field [7]:

$$\boldsymbol{B} = \nabla\psi \times \nabla(\phi - q\vartheta) \tag{1}$$

with q the safety factor[1] defined by $q(\psi) = \frac{\boldsymbol{B}.\nabla\varphi}{\boldsymbol{B}.\nabla\vartheta}$, ϑ and ϕ are respectively the poloidal and the toroidal angular coordinates. ψ is the poloidal magnetic flux normalized to 2π and stands for the radial coordinate since:

$$d\psi = -R_0 B_\theta dr, \tag{2}$$

where $\boldsymbol{B}_\theta = \nabla\psi \times \nabla\phi$ does not depend on the toroidal angle φ coordinates. This relation allows us to use indifferently the radial and the poloidal flux coordinates, then:

$$\{r, \vartheta, \phi\} \leftrightarrow \{\psi, \vartheta, \phi\}. \tag{3}$$

In the limit of large aspect ratio tokamak of major and minor radius R_0 and a, the magnetic field writes:

$$B(\psi, \vartheta) = B_{\min}(\psi)\left(1 + \frac{r(\psi)}{R_0}(1 - \cos(\vartheta)\right), \tag{4}$$

where $B_{\min}(\psi)$ is the minimal value of the magnetic field at a given ψ and at $\vartheta = 0$. Because a small system size in the ψ direction is assumed, hereafter the ψ dependence of $B_{\min}$ is neglected and $\frac{r(\psi)}{R_0}$ can be replaced by the inverse aspect ratio: $\epsilon = \frac{a}{R_0}$.

In such a configuration, trapped particles have motions with very different time-scales ($\omega_c \gg \omega_b \gg \omega_d$), where ω_c is the cyclotron frequency, ω_b the back and forth frequency (or bounce motion) and ω_d the slow toroidal precession frequency.

2.2 Trapped particle motion

The fastest motion for a charged particle is the well known cyclotron motion which is defined by its frequency, $\omega_{c,s} = \frac{|q_s|B}{m_s}$ where s stands for the species and the Larmor radius of the rotation $\rho_{c,s} = \frac{v_\perp}{\omega_{c,s}}$. It can be shown that the so-called magnetic moment $\mu = \frac{m_s v_\perp^2}{2|\boldsymbol{B}|}$ is an adiabatic invariant. The motion of the guiding center is obtained by averaging the equations over the cyclotron motion. The coordinates of the guiding-center are $\boldsymbol{x_g} = (\psi_g, \vartheta_g, \phi_g)$ and the equations of motion write:

$$\frac{d\psi_g}{dt} = v_{d\psi}(\boldsymbol{x_g}), \tag{5}$$

$$\frac{d\vartheta_g}{dt} = \frac{v_{g||}(\boldsymbol{x_g})}{q(\psi_g)R} + v_{d\theta}(\boldsymbol{x_g}), \tag{6}$$

$$\frac{d\phi_g}{dt} = \frac{v_{g||}(\boldsymbol{x_g})}{R} + v_{d\varphi}(\boldsymbol{x_g}), \tag{7}$$

with $v_{g||}$ the guiding center velocity along the magnetic field lines, and v_d the gradient and curvature drift velocity. In a tokamak plasma the kinetic pressure is much smaller than the magnetic pressure which is called the low-beta approximation. Using this approximation the gradient and curvature drift velocities can be written:

$$\boldsymbol{v_d} = \frac{m_s v_{g||}^2 + \mu|\boldsymbol{B}|}{q_s|\boldsymbol{B}|^3}(\boldsymbol{B} \times \nabla|\boldsymbol{B}|), \tag{8}$$

where $\boldsymbol{B}$ is estimated at the guiding center position $\boldsymbol{x_g}$.

We can introduce two adiabatic invariants which are derived at first order in $\rho^{\wedge 2} = \frac{\rho_{c,s}^2}{a^2}$ from the guiding-center representations of the exact invariants of particles. These invariants are the kinetic energy and the toroidal kinetic momentum:

$$E = \frac{1}{2}m_s v_{g||}^2 + \mu B(\boldsymbol{x_g}) \tag{9}$$

$$M = q_s\psi(\boldsymbol{x_g}) + m_s R(\boldsymbol{x_g})v_{g||}. \tag{10}$$

Since the total energy of a particle must remain constant, the parallel velocity must necessarily decrease as a particle moves from a weak-field region to a strong-field region. If B is large enough, the parallel velocity eventually becomes zero, and the particle is reflected back to the weak-field region. This occurs for trapped particles which satisfy: $\frac{1}{1+2\phi} < \lambda$ with $\lambda = \frac{\mu B_{\min}}{E}$. For this class of particles we can write:

$$M = q_s\psi_0, \tag{11}$$

[1] In this paper, we note q the safety factor, q_0 the safety factor at the magnetic surface ψ_0 and q_s the charge of the s species.

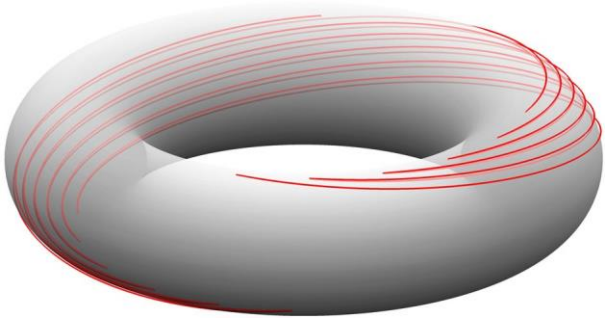

Fig. 1. Guiding-center orbit in a torus for a trapped particle.

where $\psi_0 = \psi(\boldsymbol{x_o})$ is the poloidal magnetic flux at the turning point $\boldsymbol{x_o}$. In its back and forth motion from one turning point to the other, with the frequency ω_b, a trapped particle trajectory draws a banana-like shape when projected on the poloidal cross-section. Indeed, the vertical drift, due to $v_{d\theta}$ and $v_{d\psi}$, leads to the width δ_b of this trajectory.

Finally the drift in the toroidal direction $v_{d\varphi}$ gives the third and slowest periodic motion defined by ω_d, the frequency of the bounce-averaged toroidal drift. An illustration of the toroidal precession is shown Figure 1.

2.3 Action and angular variables

A dynamical system that shows different periodic motions is the ideal framework for using action and angular variables. These coordinates will be useful to decrease the dimensionality of our system.

Taking the two variables (P, Q) that are the canonical momentum-coordinate conjugate pair describing a periodic motion, the action defined by $S = \oint P\,dQ$ is an invariant ($\frac{dS}{dt} = 0$). Note that this result can be extended for quasi-periodic motions where S is then an adiabatic invariant [8]. For trapped particles in the absence of perturbation, three periodic coordinates exist, namely the cyclotron phase ϕ_c, the poloidal and toroidale angles (ϑ, ϕ) due to bounce and precession motions. In the presence of an electric potential Φ and a magnetic vector potential $\boldsymbol{A}$, the Hamiltonian of a particle of mass m_s and electric charge q_s reads:

$$\mathrm{H} = \frac{1}{2m_s}(\boldsymbol{P} - q_s\boldsymbol{A})^2 + q_s\Phi \tag{12}$$

with $\boldsymbol{P}$ the canonical momentum. In this framework, the action-angle variables are defined as [9–11]:

$$\boldsymbol{J} = \begin{pmatrix} J_1 = -\frac{\mu}{m_s} \\ J_2 \\ J_3 = M \end{pmatrix} \quad \boldsymbol{\alpha} = \begin{pmatrix} = \omega_c(\boldsymbol{J})t + \alpha_{10} \\ \frac{q_s}{m_s v_{G\parallel}} \oint_b ds = \omega_b(\boldsymbol{J})t + \alpha_{20} \\ \alpha_3 = \omega_d(\boldsymbol{J})t + \alpha_{30} \end{pmatrix}. \tag{13}$$

Since v_g depends on energy E and J_1, J_2 is a function of deal with J_1 and E which are usual quantities [12]. In the following the sets μ, E, M and J_1, J_2, J_3 are used indifferently. Averaging over the cyclotron motion (i.e. over the variable α_1) gives the coordinates of the guiding center at the first order [9–11]:

$$\psi_g = \psi_0 + \hat{\psi}(\boldsymbol{J}, \alpha_2), \tag{14}$$

$$\vartheta_g = \hat{\vartheta}(\boldsymbol{J}, \alpha_2), \tag{15}$$

$$\varphi_g = \alpha_3 + q_0\hat{\vartheta}(\boldsymbol{J}, \alpha_2) + \hat{\varphi}(\boldsymbol{J}, \alpha_2), \tag{16}$$

Neglecting the deviation from regular precession motion $\hat{\varphi}(\boldsymbol{J}, \alpha_2)$, we note $\alpha = \alpha_3 = \varphi_g - q_0\vartheta_g$. Starting from this point, we can then calculate the bounce frequency and the precession frequency [13]:

$$\omega_{b,s} = \frac{\sqrt{2\frac{E}{m_s}}}{q_0 R_0}\bar{\omega}_b \tag{17}$$

$$\omega_{d,s} = \frac{q_0}{a}\frac{E}{q_s B_{min} R_0}\bar{\omega}_d \tag{18}$$

with

$$\bar{\omega}_b = \frac{\pi\sqrt{\epsilon}}{2\,2\mathrm{K}(\kappa^2)}$$

and

$$\bar{\omega}_d = \frac{2\mathrm{E}(\kappa^2)}{\mathrm{K}(\kappa^2)} - 1 + 4s_0\left(\frac{\mathrm{E}(\kappa^2)}{\mathrm{K}(\kappa^2)} + \kappa^2 - 1\right),$$

where $\kappa^2 = \frac{1-\lambda}{2\epsilon}$ is the pitch-angle parameter, s_0 is the magnetic shear, and $\mathrm{K}(\kappa^2)$ and $\mathrm{E}(\kappa^2)$ are the complete elliptic functions of the first kind and second kind respectively [14]. Noticably, given the charateristics of tokamak plasmas, it appears that the precession frequency of thermal particles is much smaller than their bounce frequency: $\omega_d \ll \omega_b$. The ratio is typically of the order of $q^2\rho_{c,s}/(\epsilon^{1/2}r)$, with $\epsilon = r/R_0$. That is the reason why we will average over the bounce motion (α_2) to study the dynamics at the precession time scale which corresponds to the turbulence time scale. The final model will work in the space (ψ, α) which is close to the usual (r, φ) space. The second result is that the precession drift does not depend on the mass of the particle but on its charge. Thus the ions and the electrons precess with the same frequency but in opposite directions.

3 The kinetic model for TIM + TEM

In this section, we recall the Vlasov equation for the banana particles and for the s species. The quasi neutrality constraint is derived when the response of passing particles is assumed adiabatic, while the kinetic response is retained these two invariants. Is it more convenient and easier to

for trapped particles. Finally we write the normalized set of equations of the trapped ion-electron model.

3.1 The gyro-bounce kinetic Vlasov equation

In order to derive a kinetic model describing TIM and TEM instabilities we use the gyro-average over both the cyclotron motion and the bounce motion to write the Vlasov equation for each species in the (ψ, α) phase space. At the equilibrium averaging the Hamiltonian leads to:

$$\frac{1}{q_s}\frac{\partial H_s}{\partial \psi} = \omega_{d,s} \quad \longrightarrow \quad H_s = E(1 + e\Omega_d \psi) \tag{19}$$

with $\Omega_d = \frac{\omega_{d,s} Z_s}{}$ which does not depend on ψ according to equation (18), Z_s the electric charge of the s species ($Z_e = -1$) and e is the elementary electric charge. This quantity does not depend on the species. We also assume that in the radial direction the precession frequency has a low ψ dependence. Then adding an electrostatic perturbation the Hamiltonian writes:

$$H_s = E(1 + e\Omega_d \psi) + eZ_s \mathrm{J}_{0s}\Phi(\boldsymbol{J}, \alpha) \tag{20}$$

with J_{0s} is the average operator, taking into account the difference between the non locality of the calculated electric potential for "banana" particles and the potential at the real position of the particle, a more general formulation is given by [15]. It is obvious that this operator depends on the species. Indeed the average is performed over the bounce trajectory that shows different scales according to the species. In our case, we apply the more simple approach as given in [9]. First, due to the shape of the magnetic field the fluctuating electric potential is assumed to depend on ψ and $\varphi\ q(\psi)\vartheta$ only. Then, in the limit of large wavelengths $k\delta_b \quad 1$ and $n\rho_c \quad 1$, where n (resp. k) the toroidal (resp. radial) mode number, the average operator writes:

$$\mathrm{J}_{0s} = \quad 1 + \frac{E}{T_{eq,s}}\frac{\delta_{b0,s}^2}{4}\partial_\psi^2 \qquad 1 + \frac{E}{T_{eq,s}}\frac{q_0^2\rho_{c0,s}^2}{4a^2}\partial_\alpha^2 \tag{21}$$

with

$\rho_{c0,s}$ and $\delta_{b0,s}$ the thermal Larmor radius and the thermal banana width and $T_{eq,s}$ the equilibrium temperature of the species s. Finally we consider a Pade approximation which is equivalent to the exact operator at large wavelengths and ensures the damping of small scales [10]. The average operator then writes:

$$\mathrm{J}_{0s} = \quad 1 - \frac{E}{T_{eq,s}}\frac{\delta_{b0,s}^2}{4}\partial_\psi^2 \qquad 1 - \frac{E}{T_{eq,s}}\frac{q_0^2\rho_{c0,s}^2}{4a^2}\partial_\alpha^2 \qquad . \tag{22}$$

Finally the Vlasov equation for the species s reads:

$$\frac{\partial f_s}{\partial t} - [\mathrm{J}_{0s}\Phi, f_s] + \frac{\Omega_d E}{Z_s}\frac{\partial f_s}{\partial \alpha} = 0, \tag{23}$$

with the Poisson's brackets defined by $[f, g] = \partial_\alpha f \partial_\psi g - \partial_\alpha g \partial_\psi f$. Here f_s is the bounce averaged gyro-kinetic distribution function of the species s, which represents the distribution of "banana centers". Equation (23) is the same as the one derived in reference [6]. Each species evolves according to similar Vlasov-type equations, with species-dependent expressions of the gyro-bounce operator.

3.2 Quasi-neutrality constraint

Using action-angle variables allows a very simple expression of the Hamiltonian and consequently the gyro-kinetic Vlasov equation. The price to pay is to transfer the topological difficulties to the quasi-neutrality constraint which is now more complicated. The spatial scale of the trapped particle turbulence is much larger than the Debye length ($\lambda_D^2 k^2 \quad 1$), that allows to replace Maxwell-Poisson equation by the electro-neutrality constraint $n_i = n_e$.

The first difficulty is to find the connection between the density, calculated by the integral of the distribution function over the velocity space, and the same density calculated with action-angle variables. For this purpose, by expressing and equalizing the two elementary volumes, we first write [10]:

$$d^3\alpha d^3\boldsymbol{J} = d^3x 4\pi \sqrt{2}\bar{m}_s^{-3/2} E^{1/2} dE \frac{d\lambda}{4\bar{\omega}_b}. \tag{24}$$

Noting that $m^3 d^3x d^3v = d^3\alpha d^3J$, we obtain:

$$\int_{-\infty}^{+\infty} \frac{d^3v}{(2\pi/m)^{3/2}} = \frac{2f_T}{\sqrt{\pi}} \int_0^1 \kappa \mathbb{K}(\kappa^2) d\kappa \int_0^{+\infty} E^{1/2} dE \tag{25}$$

with $f_T = \frac{}{\pi}$ the fraction of trapped particles. In order to derive the density we have to integrate the distribution function of the particles.

The second difficulty is that the Vlasov equation of the system deals with the bounce averaged gyro-kinetic distribution function. The gyro-kinetic theory helps us to write the particle density as follows [10,11]:

$$n_s = 4f_T\pi\sqrt{2}\bar{m}_s^{-\frac{3}{2}} \int_0^1 \kappa \mathbb{K}(\kappa^2) d\kappa \int_0^{+\infty} \mathrm{J}_{0s} f_s E^{1/2} dE + \frac{q_s n_{eq} f_T}{T_{eq,s}} \bar{\Delta}_s(\Phi). \tag{26}$$

The difference between the particle density and the gyro-bounce-center density corresponds to an effective polarization. The density associated to this polarization can be expressed as a Laplacian operator defined by:

$$\bar{\Delta}_s = \frac{q_0\rho_{c0,s}}{a}^2 \partial_\alpha^2 + \delta_b^2\partial_\psi^2.$$

A response of the passing particles is taken into account in our model [11]. For the fluctuating potential which have a non-zero gradient along the magnetic field (i.e. $n = 0$), the passing particle response is adiabatic. For the so called radial modes $n = 0$, a response that depends on the turbulent regime must be considered [5]. In the ion turbulence, the electrons have no response for $n = 0$, due to their small Larmor radius. On the contrary, the ion Larmor radius is larger than the electronic turbulence correlation length, therefore in this case the response of ions remains adiabatic for radial modes.

Nevertheless, because the model can describe all regimes of turbulence, the response of passing particles for

radial mode will have an intermediate behavior between no response and an adiabatic response. Therefore, we introduce the parameter λ_s ($0 < \lambda_s < 1$ = adiabatic) which describes the impact of the species response to the radial modes. Thus the density fluctuation of passing particles can be written:

$$\frac{n_{s,p}}{n_{eq}} = -\frac{(1-f_T)q_s}{T_{eq,s}}(\Phi - \lambda_s\langle\Phi\rangle). \quad (27)$$

Finally, the quasi-neutrality equation reads:

$$\frac{2}{\sqrt{\pi}}\frac{1}{n_{eq}}\left[\int_0^{+\infty} J_{0i} f_i E^{1/2} dE - \left(\frac{m_e}{m_i}\right)^{-\frac{3}{2}}\int_0^{+\infty} J_{0e} f_e E^{1/2} dE\right] = -\frac{e}{T_{eq,i}}\left[\bar{\Delta}_i(\Phi) + \tau\bar{\Delta}_e(\Phi)\right] + (1-f_T)\frac{(1+\tau)e}{T_{eq,i} f_T}(\Phi - \epsilon_\phi\langle\Phi\rangle) \quad (28)$$

with $\tau = \frac{T_{eq,i}}{T_{eq,e}}$ and $\epsilon_\phi = \frac{\lambda_i + \tau\lambda_e}{(1+\tau)}$. For the sake of simplicity, we assume that $\int_0^1 \kappa K(\kappa^2)d\kappa \sim 1$. The quasi neutrality exhibits the same structure as in reference [6]. The main difference comes from the adiabatic term $(\phi - \bar{\phi})$ which appears in the model in reference [6] to describe passing particles and trapped electrons, whereas only passing particles are adiabatic in this paper.

3.3 Normalization

The energy is normalized to a typical thermal energy T_0, the time to a reference frequency ω_0, the lengths are normalized to the radial size of the box in units of ψ and the electric potential to $\omega_0 L_\psi$, with $L_\psi = a\frac{d\psi}{dr} = aR_0 B_\theta$

$$\hat{E} = \frac{E}{T_0}, \quad \hat{t} = \omega_0 t, \quad \hat{\psi} = \frac{\psi}{L_\psi}, \quad \hat{\Phi} = \frac{\Phi}{\omega_0 L_\psi}. \quad (29)$$

The system then writes:

$$\begin{cases} \frac{2}{\sqrt{\pi}}\left[\int_0^{+\infty} J_{0i} f_i \hat{E}^{1/2} d\hat{E} - \int_0^{+\infty} J_{0e} f_e \hat{E}^{1/2} d\hat{E}\right] = C_{ad}(\hat{\Phi} - \epsilon_\Phi\langle\hat{\Phi}\rangle) - C_{pol}\left[\bar{\Delta}_i(\hat{\Phi}) + \tau\bar{\Delta}_e(\hat{\Phi})\right] \\ \frac{\partial f_e}{\partial\hat{t}} - \left[J_{0e}\hat{\Phi}, f_e\right] - \hat{E}\hat{\Omega}_d\frac{\partial f_e}{\partial\alpha} = 0 \\ \frac{\partial f_i}{\partial\hat{t}} - \left[J_{0i}\hat{\Phi}, f_i\right] + \hat{E}\hat{\Omega}_d\frac{\partial f_i}{\partial\alpha} = 0 \end{cases} \quad (30)$$

with $\hat{\Omega}_d = \frac{\Omega_d T_0}{\omega_0}$, $C_{pol} = \frac{e\omega_0 L_\psi}{T_0}$ and $C_{ad} = \frac{C_{pol}(1+\tau)(1-f_T)}{f_T}$.

For the sake of clarity of reading, hereafter the notation "^" is no longer used.

4 Linear analysis of the system

4.1 Getting the dispersion relation

With the aim of deriving the dispersion relation from the set of equation (30) for TIM and TEM modes, we let $\boldsymbol{E} = \boldsymbol{0}$ at the equilibrium. In zeroth and first orders, the distribution functions and the electrostatic potential write:

$$f_s = F_{eq,s} + \tilde{f}_s, \qquad \Phi = \tilde{\Phi}. \quad (31)$$

The linearization assumes retaining only terms up to first order, so that the term $[J_{0s}\tilde{\Phi}, \tilde{f}_s]$ in the Vlasov equation will be neglected. The fluctuations are assumed to be of the form:

$$\tilde{f}_s = \sum_{n,\omega} f_{s,n,\omega}(\psi)e^{i(n\alpha - \omega t)}, \quad (32)$$

$$\tilde{\Phi} = \sum_{n,\omega} \Phi_{n,\omega}(\psi)e^{i(n\alpha - \omega t)}. \quad (33)$$

Using the usual Landau prescription on the imaginary part of ω, the system writes:

$$f_{s,n,\omega}(\psi) = \frac{n\left[\kappa_n + \kappa_T\left(\frac{E}{T} - \frac{3}{2}\right)\right]}{Z_s^{-1} n\Omega_d E - \omega} J_{n,s}\Phi_{n,\omega}(\psi) F_{eq,s}$$

$$C_n\Phi_n = \frac{T_{eq}^{\frac{5}{2}}}{n_{eq}}\sum_s\int_0^\infty J_{n,s} f_{n,s}\left(\frac{E}{T_{eq}}\right)^{\frac{1}{2}}\frac{dE}{T_{eq}} \quad (34)$$

with

$$C_n = \frac{\sqrt{\pi}}{2}\left[C_{ad} + C_{pol}\left(n^2(\rho_{c,i}^2 + \rho_{c,e}^2) + k^2(\delta_{b,i}^2 + \delta_{b,e}^2)\right)\right]$$

that contains the coefficients corresponding to the passing particles, the polarization term and $\kappa_{n,T}^{-1} = (\partial_\psi \log(n_{eq}, T_{eq}))^{-1}$ the density and the thermal gradient lengths. Here the gradients and the equilibrium temperature are assumed to be the identical for both species. Thus, the dispersion equation writes:

$$D = C_n - \int_0^\infty \frac{\kappa_n + \kappa_T\left(\xi - \frac{3}{2}\right)}{\Omega_d(\xi - x)} J_{n,i}^2 e^{-\xi}\xi^{\frac{1}{2}}d\xi - \int_0^\infty \frac{\kappa_n + \kappa_T\left(\xi - \frac{3}{2}\right)}{\Omega_d(\xi + x)} J_{n,e}^2 e^{-\xi}\xi^{\frac{1}{2}}d\xi \quad (35)$$

with $\xi = \frac{E}{T_{eq}}$, $x = \frac{\omega}{(nT_{eq}\Omega_d)}$. The first integral on the right hand side, driven by the ion dynamics, shows that the resonance between wave and ions occurs when the phase velocity has the same sign as the ionic precession drift (i.e. $\omega > 0$). Similarly, the resonance between the electrons and wave occurs when the phase velocity has the same sign as the electronic precession drift (i.e. $\omega < 0$).

The stability of the system can be found by deriving the stability threshold in the (κ_n, κ_T) plane, for which $\gamma = \mathrm{Im}(\omega) = 0$.

Note that in order to determine the instability growth rate we will focus on the area where instabilities can occur, i.e. for which $\mathrm{Im}(\gamma) > 0$. Since the real axis is never

Table 1. Main parameters used for the linear analysis.

$\delta_{b,i}$	$\delta_{b,e}$	$\rho_{c,i}$	$\rho_{c,e}$	c_n	$\hat{\Omega}_d$	T_eq	k
0.1	2×10^{-3}	0.01	2×10^{-4}	0.1	1	1	1

crossed, the function $\sqrt{x}$ can be trivially used. In this case, taking $F_s(\xi) = \kappa_n + \kappa_T \left(\xi - \frac{3}{2}\right) J^2_{n,s}(\xi)$ the equation (35) can be written:

$$D(\omega) = C_n \left[\int_0^\infty \frac{F_i(\xi) - F_i(x)}{(\xi - x)} \sqrt{\xi}\, d\xi - F_i(x)\sqrt{\pi}\left(1 + \sqrt{x}Z(\sqrt{x})\right) - F_e(-x)\sqrt{\pi}\left(1 + i\sqrt{x}Z(i\sqrt{x})\right) - \int_0^\infty \frac{F_e(\xi) - F_e(-x)}{(\xi + x)} e^{-\xi}\sqrt{\xi}\, d\xi \right] = 0 \quad (36)$$

with $Z(x) = \pi^{-\frac{1}{2}} \int_{-\infty}^{+\infty} \frac{e^{-t^2}}{t-x} dt$ the plasma dispersion function defined by Fried and Conte [16]. Note that for $x \in$ [17] gives

$$Z(x) = e^{-x^2}\left[i\pi^{\frac{1}{2}} - 2\int_0^x e^{t^2} dt\right]$$

$$Z(ix) = i\pi^{\frac{1}{2}} e^{x^2} \mathrm{erfc}(x) \quad (37)$$

with erfc(x) the complementary error function. Note that, close to the resonance in (36) the term $\frac{F_s(\xi) - F_s(\pm x)}{(\xi \pm x)}$ does not diverge and goes to the ξ derivative of F_s.

4.2 Solutions, trapped ion and trapped electron modes

In this section, the dispersion relation is solved by scanning the (ω_r, γ) plane, looking for values of $\omega = \omega_r + i\gamma$ such that the dispersion function vanishes within machine precision. For this purpose a method that finds the minimum of a scalar function of several variables, starting at an initial state, and uses the simplex search method [18], is used. Among these solutions one finds the couple (ω_r, γ) for which the instability growth rate is maximum. All results presented in this section are obtained with the plasma parameters given in Table 1.

In Figures 2 and 3 the linear growth rate and the real frequency for ($\kappa_n = 0$, $\kappa_T = 0.25$) are plotted against n. Note that for $\kappa_n = 0$ the marginal solutions are trivial. Indeed equation (35) shows that the imaginary part of the dispersion relation vanishes for $x \equiv \frac{\omega}{n\Omega_d} = \pm\frac{3}{2}$ [9]. In Figure 2, we observe that the negative pulsation (in the electronic precession direction) and the positive pulsation (in the ionic precession direction) are in good agreement with the curve $\omega_r = \pm\frac{3}{2}n$. Figure 3 shows that for low toroidal mode numbers n both species can be destabilized, whereas only TEM modes are unstable for large n. This agrees well with the behavior of the gyro average operator which depends on ρ_c and n.

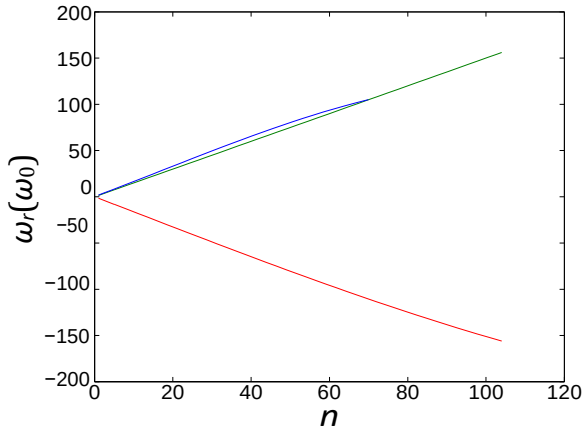

Fig. 2. Real frequency of the trapped electron (resp. ion) modes in red (resp. in blue) plotted against the toroidal mode number n. The green line is $\omega = \frac{3}{2}n$ and corresponds to the marginal TIM mode [9].

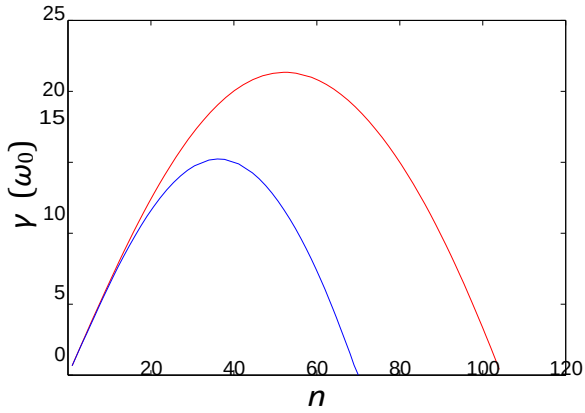

Fig. 3. Linear growth rates of the trapped electron (resp. ion) modes in red (resp. in blue) plotted against n.

The absolute linear instability threshold is plotted in Figure 4 as a function of κ_n and κ_T beyond which there is at least one unstable mode. For $\kappa_n > 0$, this threshold is equivalent to the diagram of instability threshold for the mode $n = 1$. On the other side of the plane ($\kappa_n < 0$), the threshold is obtained by scanning the stability diagram over mode number n.

It is interesting to observe which kind of instability (TIM or TEM) occurs beyond this threshold. In Figures 5 and 6 the diagrams of instability threshold for $n = 40$ and $n = 100$ are shown. For $n = 40$ the instability diagram shows three distinct zones. The stable region where no instability can occur, obviously contains the point ($\kappa_n = 0, \kappa_T = 0$). Based in Figures 2 and 3, we can conclude that the top area presents two roots, both species developing an instability. Between these two regions, one area where only trapped electrons can develop an instability exists. We notice that TEM shows a lower instability threshold than TIM, which is in agreement with what is expected [5,19]. For largest toroidal mode numbers, b_i is close to zero and only TEM instability is expected. This is in agreement with the result shown in Figure 6, where only stable and

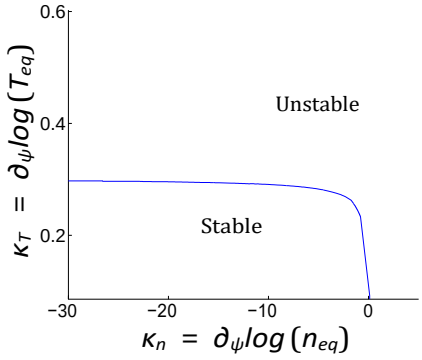

Fig. 4. Absolute linear instability threshold as a function of κ_n and κ_T with the parameters listed in Table 1.

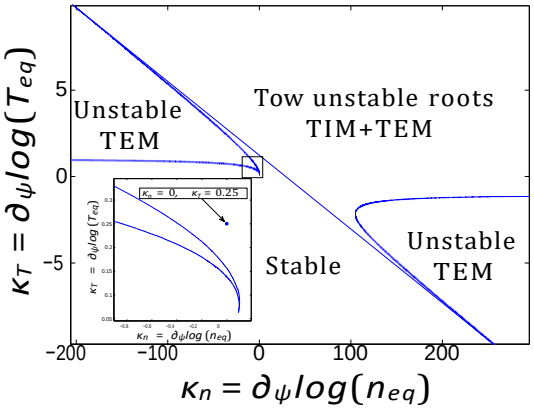

Fig. 5. Linear instability threshold as a function of κ_n and κ_T for $n = 40$.

unstable regions driven by trapped electron modes can be distinguished.

Usually, it is expected that the ion instability is dominant [19]. On this regime, the instability threshold is expected to be lower at low values of κ_n. Indeed an increase of κ_n has an stabilizing effect [20]. The above results show a completely different situation where the TEM instability is dominant. This result is due to the fact that the model only deals with TEM and TIM modes and that ITG instabilities due to passing particles are not taken into account.

5 Conclusion

The trapped ion and electron driven modes have been studied by solving linearly a Vlasov equation averaged over the cyclotron and bounce motion of trapped particles. This model allows to reduce the dimensionality of the dynamical system. The distribution function depends on the radial coordinate and the precession angle of trapped particles and is parametrized by the energy and pitch angle.

The accuracy of the model has been verified with an exact solution in the marginal case. In a next work the effects of the passing ions will be studied by artificially reducing the electron response. The next step is to perform nonlinear investigations. Moreover, in order to study the effect of trapped electron, a kinetic electron response

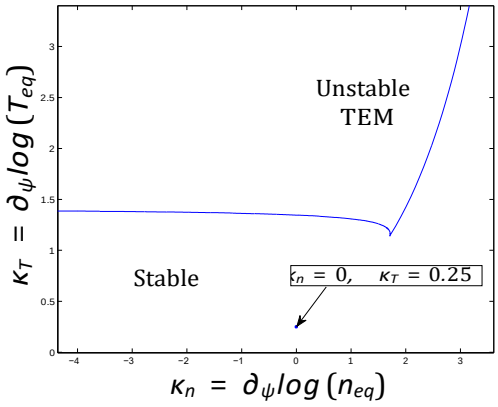

Fig. 6. Linear instability threshold as a function of κ_n and κ_T for $n = 100$.

will be implemented in the nonlinear semi-lagrangian TERESA code [21,22]. The study of the nonlinear interactions between TEM and TIM modes will be investigated.

This work was carried out within the framework the European Fusion Development Agreement and the French Research Federation for Fusion Studies. It is supported by the European Communities under the contract of Association between Euratom and CEA. The views and opinions expressed herein do not necessarily reflect those of the European Commission.

References

1. W. Horton, Rev. Mod. Phys. **71**, 735 (1999)
2. L. Villard et al., Nucl. Fusion **44**, 172 (2004)
3. X. Garbet, Plasma Phys. Control. Fusion **43**, 251 (2001)
4. T. Dannert, F. Jenko, Phys. Plasmas **12**, 072309 (2005)
5. X. Garbet et al., Nucl. Fusion **50**, 043002 (2010)
6. A. Ghizzo et al., Transport Theo. Stat. Phys. **40**, 382 (2011)
7. A.H. Boozer, Rev. Mod. Phys. **76**, 1071 (2004)
8. P. Bellan, in *Fundamentals of Plasma Physics* (Cambridge University Press, 2006), p. 75
9. G. Depret et al., Plasma Phys. Control. Fusion **42**, 949 (2000)
10. Y. Sarazin et al., Plasma Phys. Control. Fusion **47**, 1817 (2005)
11. A. Ghizzo et al., Phys. Plasmas **17**, 092501 (2010)
12. X. Garbet et al., J. Comput. Phys. **87**, 249 (1990)
13. B. Kadomtsev, O.P. Pogutse, Rev. Plasma Phys. **5**, 249 (1970)
14. M. Abramowitz, A. Stegun, in *Handbook of mathematical functions* (Dover Publications, 1964), p. 590
15. L. Wang et al., Phys. Plasmas **16**, 062309 (2010)
16. B.D. Fried, S.D. Conte, *The Plasma Dispersion Function* (Academic Press, New York, 1961)
17. J.D. Huba, in *Naval Research Laboratory Plasma Formulary* (The office of Naval Research, 2011), p. 30
18. J.C. Lagarias et al., SIAM J. Opt. **9**, 112 (1998)
19. F. Romanelli, S. Briguglio, Phys. Fluids B **2**, 754 (1990)
20. F. Romanelli, Phys. Fluids B **5**, 1018 (1989)
21. T. Cartier-Michaud et al., ESAIM Proc. **43**, 274 (2013)
22. J. Abiteboul et al., ESAIM Proc. **32**, 103 (2011)